AIAA 92-0110

Secondary Drop Breakup in the Deformation Regime

L.-P. Hsiang and G. M. Faeth
The University of Michigan
Ann Arbor, MI

30th Aerospace Sciences Meeting & Exhibit
January 6-9, 1992 / Reno, NV

Secondary Drop Breakup in the Deformation Regime

by

L.-P. Hsiang* and G. M. Faeth†
Department of Aerospace Engineering
The University of Michigan
Ann Arbor, MI 48109-2140

Abstract

The properties of drop deformation and secondary breakup were observed for shock wave initiated disturbances in air at normal temperature and pressure. Test liquids included water, glycerol solutions, n-heptane and mercury to yield Weber numbers of 0.5-1000, Ohnesorge numbers of 0.0006-4, liquid/gas density ratios of 580-12000 and Reynolds numbers of 300-16000. Measurements included pulsed shadowgraphy and holography to find drop deformation properties prior to breakup as well as drop size distributions after breakup. Drop deformation and breakup regimes were identified in terms of Weber and Ohnesorge numbers: regimes at low Ohnesorge numbers include no deformation, nonoscillatory deformation, oscillatory deformation, bag breakup, multimode breakup and shear breakup as the Weber number is increased. However, these regimes become restricted to higher Weber numbers at large Ohnesorge numbers, with no breakup observed for Ohnesorge numbers greater than 4 over the present test range. Unified temporal scaling of deformation and breakup processes was observed in terms of a characteristic breakup time that largely was a function of Ohnesorge number. Prior to breakup, the drag coefficient evolved from the properties of spheres to those of thin disks as drop deformation progressed. The drop size distribution after breakup satisfied Simmons' universal root normal distribution function and could be characterized by the Sauter mean diameter (SMD) alone. The SMD after secondary breakup could be correlated in terms of a characteristic liquid boundary layer thickness for all breakup regimes, similar to recent results for nonturbulent primary breakup. Drop properties after secondary breakup suggest potential for additional breakup of the larger drops formed when relative velocities are high.

Nomenclature

C_D	= drop drag coefficient
C_f	= empirical constant for deformation forces, Eq. (5)
C_s	= empirical constant for SMD, Eq. (12)
C_v	= empirical constant for drop volume, Eq. (6)
d	= drop diameter
d_c	= crosstream diameter of drop
d_s	= streamwise diameter of drop
D	= drop drag force
MMD	= mass median diameter
Oh	= Ohnesorge number, $\mu_f/(\rho_f d_o \sigma)^{1/2}$
Re	= Reynolds number, $\rho_g d_o u_o/\mu_g$
SMD	= Sauter mean diameter
t	= time
t_b	= drop breakup time
t^*	= characteristic breakup time, $d_o(\rho_f/\rho_g)^{1/2}/u_o$
t_c^*	= corrected characteristic breakup time, Eq. (4)
u	= streamwise relative velocity
u_f	= characteristic liquid velocity, $(\rho_g/\rho_f)^{1/2}u_o$
x	= streamwise position of drop centroid
δ	= liquid boundary layer thickness
μ	= molecular viscosity
ρ	= density
σ	= surface tension

Subscripts

f	= liquid-phase property
g	= gas-phase property
max	= maximum value
min	= minimum value
o	= initial condition

Introduction

Secondary breakup of drops is an important multiphase flow process with applications to liquid atomization, dispersed multiphase flow, combustion instability of sprays, heterogeneous detonations of gas/liquid mixtures, the properties of rain, and interactions between high-speed aircraft and rain, among others. In particular, recent studies of the structure of dense pressure-atomized sprays, see Refs. 1 and 2 and references cited therein, confirm the conventional view of liquid atomization with primary breakup at the liquid surface followed by secondary breakup. It also was found that secondary breakup can control mixing rates of dense sprays in some instances, much like drop vaporization often controls mixing rates of dilute sprays. Additionally, recent studies of primary breakup of both nonturbulent and turbulent liquids show that primary breakup intrinsically yields drops that are unstable to near-limit secondary breakup.[3,4] Motivated by these observations, the objectives of the present investigation were to study drop deformation and breakup for well-defined shock wave disturbances (yielding a step change in the relative velocity of a drop) at conditions near the onset of secondary breakup. Issues considered include required flow conditions, dynamics and outcomes of drop deformation and breakup.

Due to numerous applications, secondary breakup has received significant attention in the past. Giffen and Muraszew[5] and Hinze[6] review early work in the field; therefore, the following discussion will be limited to more recent studies. The definition of the onset of breakup, breakup dynamics and the outcome of breakup will be considered, in turn. Most earlier work has at least touched on the definition and conditions for the onset of various breakup regimes.[5-21] The breakup regime observed at the onset of secondary breakup has been termed bag breakup: it involves deflection of the drop into a thin disk normal to the flow direction, followed by deformation of the center of the disk into a thin balloon-like structure extending in the downstream direction (see Refs. 6,9,14,17-21 for photographs of all the breakup regimes discussed here). The shear breakup regime is observed at higher relative velocities: it involves deflection of the periphery of the disk in the downstream direction, rather than the center, and stripping of drops from the periphery of the disk. The transition between the bag and shear breakup regimes involves complex breakup processes, with portions of this regime termed parachute breakup,[16] chaotic breakup,[16] bag-jet breakup,[17] transition breakup,[17] etc.; this regime will be denoted the multimode breakup regime in the following. A

* Graduate Assistant, Department of Aerospace Engineering, The University of Michigan, Ann Arbor, Michigan, 48109-2140.
† Professor, Department of Aerospace Engineering, The University of Michigan, Ann Arbor, Michigan, 48109-2140. Fellow AIAA.

complex breakup mechanism also has been observed at very large relative velocities, which is called the catastrophic breakup regime.[19,20]

Existing observations of secondary breakup have generally involved $\rho_f/\rho_g > 500$ and $Re > 100$. For these conditions, Hinze[6] has shown that transitions between breakup regimes are largely functions of the Weber number, $We = \rho_g d_o u_o^2/\sigma$, and the Ohnesorge number, $Oh = \mu_f/(\rho_f d_o \sigma)^{1/2}$, which are measures of the ratios of drag and liquid viscous forces to surface tension forces, respectively. He found that progressively larger disturbances, larger We, were required for the onset of breakup as Oh increased because viscous forces in the liquid tend to inhibit drop deformation at large Oh, which is the first step in the breakup process. In fact, viscous forces essentially suppressed secondary breakup for the available range of We, for $Oh > 2$.[6] Among others, Loparev[15] showed that the properties of the disturbances also affected the onset of breakup, with more slowly applied disturbances requiring higher values of We for breakup at a particular value of Oh: subsequent considerations will be limited to shock wave disturbances. Borisov, et al.[16] proposed an alternative breakup regime map in terms of We and Re, considering both the bag and shear breakup regimes, which is best suited to conditions where $Oh << 1$. Krzeczkowski[17] extended the breakup regime map of Hinze[6] to locate transitions to the bag, bag jet, multimode (called transition breakup) and shear breakup regimes as a function of We and Oh. Nevertheless, in spite of its importance for initiating breakup, conditions for onset of drop deformation, and the definition of deformation processes, have not received much attention.

Another aspect of secondary breakup that has been studied is the time required to complete breakup. Liang et al.[22] summarize past measurements of breakup times, including the findings of Simpkins and Bales[13] and Ranger and Nicholls[18] for shear breakup, and Reinecke and coworkers[19,20] for catastrophic breakup — all for shock wave disturbances at large ρ_f/ρ_g and low Oh. For these conditions, breakup times could be normalized by a characteristic breakup time, $t^* = d_o(\rho_f/\rho_g)^{1/2}/u_o$, finding that the normalized breakup time does not vary greatly over the large range of We that includes both the shear and catastrophic breakup regimes. However, results near the onset of secondary breakup, within the bag breakup regime, have not been studied very much in spite of the importance of these near-limit conditions to processes within practical sprays.[1-4]

The deformation properties of drops prior to secondary breakup due to shock wave disturbances have been studied for large ρ_f/ρ_g and $Oh < 0.1$. Wierzba and Takayama[21] summarize past work in this area, which included results of Ranger and Nicholls[18] and Reinecke and coworkers[19,20] for shear and catastrophic breakup, as well as their own measurements of deformation prior to shear breakup. They find that deformation scales in terms of t*, although in contrast to breakup times, the behavior of deformation during shear breakup differs somewhat from catastrophic breakup. Additionally, they highlight problems of interpreting shadowgraph photographs of breakup processes and suggest use of holography instead. Similar to breakup times, however, drop deformation within the bag and transition breakup regimes have not received much attention.

Finally, due to the problems of observing drops after secondary breakup, there is very little information available about the outcome of secondary breakup even though this information is vital for understanding the structure of dense sprays.[2] An exception is some limited results reported by Gel'fand et al.[14] for the bag breakup regime. A bimodal distribution was observed with small drops resulting from breakup of the bag and a group of larger drops associated with breakup of the liquid ring at the base of the bag. However, this information is too limited to provide general guidance about drop sizes produced by secondary breakup.

The preceding review indicates that there are several gaps in the literature concerning secondary breakup. In particular, conditions for the onset of various breakup regimes have been defined reasonably well by Krzeczkowski[17] but analogous deformation regimes have not been defined, particularly at high Oh where liquid viscosity effects are important. Breakup times and drop deformation have been studied as well,[18-20] however, available information is limited for the bag and transition breakup regimes that are important for drop breakup in dense sprays. Finally, measurement problems have limited information on the outcome of secondary breakup so that virtually no information is available for this critical breakup property. Thus, the objectives of the present investigation were to extend the earlier work to provide measurements of the onset of various deformation and breakup regimes, the evolution of breakup processes, and the resulting drop sizes after secondary breakup. Phenomenological descriptions of these processes were used to help interpret the data. Measurements emphasized conditions near the onset of breakup where past information is very limited even though this region is particularly important for understanding the structure of dense sprays. The measurements involved pulsed shadowgraph photography and holography, the latter being particularly useful for finding drop sizes after secondary breakup. The study was limited to conditions similar to those treated by Hinze[6] and Krzeczkowski[17] which are representative of sprays near atmospheric pressure conditions: $\rho_f/\rho_g > 500$ and $Re > 100$. Shock wave disturbances were considered with water, n-heptane, mercury and various glycerol mixtures used as test liquids in order to study effects of liquid phase properties.

The paper begins with a discussion of experimental methods. Results are then considered, treating breakup regimes, breakup times, drop deformation, drop drag and drop sizes after breakup, in turn.

Experimental Methods

Apparatus

A sketch of the experimental apparatus appears in Fig. 1. A shock tube with the driven section open to the atmosphere, similar to Ranger and Nicholls,[18] was used to generate shock wave disturbances. The driver section was pressurized with air and was round with an inside diameter of 75 mm and a length of 3.1 m. The driven section had a rectangular interior crossection (38 mm wide × 64 mm high) to facilitate visualization of the flow at the test location. A transition section, with the shock tube diaphragm at its downstream end, provided a gradual evolution from the round driver section to the rectangular driven section. The driven section was 6.7 m long with the test location 4.0 m from the downstream end. This arrangement provided test times of 17-21 ms in the uniform flow region between the shock wave passing the test location and the subsequent arrival of disturbances from the contact surface and reflections from the ends of the shock tube. Test conditions involved relatively weak shock waves having shock Mach numbers of 1.01-1.24; therefore, thin Mylar film (having thicknesses of 19, 25 and 38 μm) was used for the diaphragm between the driver and driven sections of the shock tube. The Mylar film diaphragm was ruptured to initiate operation of the shock tube by heating a fine resistance wire mounted on the film: this provided a clean break of the diaphragm that was otherwise problematical because pressure differences across the diaphragm were small since the shock waves were weak.

The strength of the shock waves was monitored by two piezoelectric pressure transducers (PCB Piezotronics, Inc., Model 101A05) mounted 660 and 310 mm upstream of the test location. The outputs of these transducers were recorded using a digital oscilloscope (LeCroy, Model 9400A). The time of passage of the wave between the two transducers provides the shock Mach number (whose properties were checked for

consistency using the pressure ratio across the wave). Because of the time required to break the diaphragm with the heater wire was not very reproducible, the pressure signals were used to synchronize data accumulation from the experiment.

The drop generator system is illustrated in Fig. 2. The generator involves a vibrating capillary tube, similar to Dabora,[23] to generate a stream of drops and a drop selection system, similar to Sangiovanni and Kestin,[24] to vary the spacing between drops. The test liquid was placed in a reservoir and pressurized with air so that it flowed to the vibrator chamber and then through a capillary tube (20, 23 or 25 gage needles, 12 mm long, depending on the test condition). The upper end of the vibrator chamber was mechanically attached to a speaker (Realistic, Model 40-1319) which, in turn, was driven by a signal generator (BK-Precision, Model 3020). By varying the liquid flow rate and the frequency of vibration, a uniformly spaced stream of monodisperse drops was generated by Rayleigh breakup.[18,23] This drop stream passed through 6 mm diameter holes in the top and bottom of driven section, crossing the central plane of the driven section at the test location. Quartz windows (25 mm high × 305 mm long and mounted flush with the inside walls of the driven section) allowed observation of the interaction between the uniform gas flow behind the shock wave and the drop stream.

The separation between drops at the center of the test location from operation of the vibrating capillary tube alone was 3-4 mm, which was sufficient to allow observation of drop deformation in the early stages of bag and multimode breakup, as well as the shear breakup process, without interactions between drops. However, it was necessary to increase the spacing between drops to observe the later stages and outcomes of bag and multimode breakup. This was accomplished using the approach of Sangiovanni and Kestin,[24] by charging every other drop in the flow and electrostatically deflecting the charged drops out of the drop stream crossing the shock tube. This yielded a drop spacing of roughly 7 mm which assured the presence of drops in the region of observation when film records were made while minimizing interactions between drops.

Instrumentation

Pulsed Shadowgraphy. Drops were observed in two ways: pulsed shadowgraph photographs and motion pictures to observe the overall dynamics of breakup, and single pulse holography to observe the outcome of breakup. Initial work involved pulsed shadowgraph photography using a Xenon Corp. Micropulser (Model 457A, 10J optical power per pulse with a pulse duration of roughly 1 μs). The lamp output was collimated and directed through one of the windows at the test location. The image was recorded through the other window using a Graphlex camera (4 × 5 inch film format, Polaroid Type 55 film) at magnification of 6:1. The photographs were obtained in a darkened room, varying the time delay between the shock wave passing the downstream pressure transducer and the time of the flash so that various portions of the breakup process could be observed from repeated tests (at least two photographs were obtained for each test condition and delay time).

Pulsed shadowgraph photography was tedious for accumulating data on drop breakup over the wide range of conditions of the present investigation; therefore, the bulk of the results were obtained using motion picture shadowgraphs within a darkened room. This involved using a 20W copper vapor laser as the light source (Metalaser Technologies, Model 2051, 2 mJ per pulse, 30 ns pulse duration) and a 35 mm drum camera (Cordon, Inc., Model 351 using AGFA 10E75HDNAH film) to record the images at unity magnification. Prior to measurements, the laser was operated in the continuous pulsing mode to reach proper operating temperatures, and the camera drum was brought to proper speed with the camera shutter closed. Laser operation then was terminated briefly, the camera shutter was opened and the shock tube diaphragm was broken. As the shock wave approached the test location, detected by the pressure transducers, the laser was fired as a high frequency burst (controlled by a Hewlett-Packard Model 3314 function generator) to capture the breakup process on the film (laser frequency of 6-8 kHz for 20 pictures). The time between film records was known by monitoring the signal generator frequency with a digital oscilloscope The film records were analyzed using a Gould FD 5000 Image Display which will be described subsequently. The procedure was to obtain several (5-14) motion picture shadowgraphs for a particular test conditions. The data were then grouped to obtain statistically significant results as ensemble averages. The experimental uncertainties of the various measurements will be taken up when the results are discussed.

Holography. The holocamera and reconstruction systems used to measure drop properties after breakup were similar to earlier work in this laboratory.[1,3,4] An off-axis arrangement was used with optics providing a 2-3:1 magnification of the hologram image itself, coupled with reconstruction optics that allowed drop diameters as small as 25 μm to be measured with 5% accuracy and objects as small as 12-15 μm to be observed. The properties of the reconstructed sprays were analyzed using the Gould FD 5000 image display system with a field of view of 1.7 × 2.0 mm. Various locations in the hologram reconstructions could be observed by traversing the hologram in two directions and the video camera of the display system in the third direction.

Drops and other ellipsoidal objects were sized by measuring their maximum and minimum diameters through the centroid of the image. Assuming ellipsoidal shapes, the diameter of these objects was taken to be the diameter of a sphere having the same volume, $d^3 = d_{min}{}^2 d_{max}$. More irregular objects were sized by finding the area and perimeter of their image and computing the maximum and minimum diameters of an ellipsoid matching these properties: given these parameters, d was found as before. Results at each condition were summed over at least three realizations, considering 150-300 liquid elements, to provide drop size distributions, the mass median diameter (MMD) and the Sauter mean diameter (SMD). Experimental uncertainties generally were dominated by finite sampling limitations because each breakup event only yields a limited number of drops. Within the limitations of the definition of drop sizes, which is difficult to quantify, estimated experimental uncertainties (95% confidence) of MMD and SMD are less than 40%.

Test Conditions

Test conditions are summarized in Table 1. Test drops of water, n-heptane, mercury and various glycerol mixtures were used to provide a wide range of liquid properties. The liquid properties listed in Table 1 were obtained from Lange,[25] except for the surface tension of glycerol mixtures which were measured in the same manner as Wu et al.[3] Initial drop diameters were in the range 500-1550 μm, dictated by the need for measurable drop properties after breakup and the difficulties of producing small drops with very viscous liquids. Ranges of other variables are as follows: ρ_f/ρ_g of 580-12000, Oh of 0.0006-4, We = 0.5-1000 and Re of 300-16000. Although the full range of Oh was considered for measurements of deformation and breakup regime transitions and dynamics, measurements to find the outcome of breakup were limited to Oh < 0.1. The We range includes processes from no deformation into the shear breakup regime that are of interest to processes within dense sprays,[2] but does not reach the catastrophic breakup regime studied by Reinecke and coworkers.[19,20] As noted earlier, the Re range of present experiments is higher than conditions where gas viscosity plays a strong role in drop drag properties; within the present Reynolds number range, the drag for spheres only varies in the

range 0.6-0.4.[2,25] Shock Mach numbers were relatively low, 1.01-1.24, so that physical properties within the uniform flow region were not significantly different from room air.

Results

Deformation and Breakup Regimes

The presentation of results will begin with definition of deformation and breakup regime transitions in order to help organize the remainder of the findings. The deformation and breakup regime map, showing transitions as functions of We and Oh similar to Hinze[4] and Krzeczkowski,[17] is illustrated in Fig. 3. Present evaluation of the onset of breakup (the transition to the bag breakup regime) is essentially identical to the findings of Hinze[6] and Krzeczkowski[17] within experimental uncertainties. Present results also agree quite well with transitions found by Krzeczkowski[17] to shear breakup and multimode breakup (called transition breakup in Ref. 17). In view of the somewhat subjective identifications of breakup regimes and their transitions, this level of agreement is quite satisfying.

Observations of transitions to nonoscillatory and oscillatory deformation illustrated in Fig. 3 have not been reported before. The present definition of transition to the nonoscillatory deformation was taken to be the condition where the drop deformed so that the ratio of its maximum (crosstream) dimension to its initial diameter was 1.1, corresponding to a deformation 10%. Following this transition, there was a range of We at each Oh where the drop decayed back to a spherical shape much like an overdamped oscillation, yielding nonoscillatory deformation (defined as conditions where the second peak of the diameter fluctuation involved deformations less than 10%). For Oh > 0.4, this regime ended by the onset of bag breakup, however, for Oh < 0.4, there was a range of We where the drop oscillated with progressively decaying ratios of maximum to initial diameters before the bag breakup regime was reached: this regime is denoted the oscillatory deformation regime in Fig. 3.

The most striking feature of the flow regime map illustrated on Fig. 3 is that progressively higher We are needed for the various transitions as Oh increases. Hinze[6] and Krzeczkowski[17] also noted this effect for the breakup transitions but the behavior is similar for the deformation transitions as well, with the oscillatory deformation regime disappearing entirely for Oh > 0.4 as noted earlier. Hinze[6] concluded that breakup might no longer be observed for Oh > 2, however, it appears that Oh would have to be somewhat greater than 4, the highest value reached during the present investigation, before breakup would be inhibited for We < 1000, with somewhat higher values of Oh required to inhibit deformation for We > 1000.

Recalling that Oh characterizes the ratio between liquid viscous forces and surface tension forces, the inhibition of deformation and breakup at large Oh clearly is due to increased damping by liquid viscous forces. This slows the deformation process so that drag forces can reduce relative velocities, and the potential for breakup. Another factor is that final breakup into drops involves Rayleigh type breakup processes which become weak when the Oh is large, so that the drops tend to deform into very long cylindrical threads which exhibit little tendency to divide into drops (at least within the deformation regime). This high Oh regime is encountered during spray combustion processes at high pressures, where values of surface tension become small but viscosity remains finite as the drop surface nears its thermodynamic critical point. Thus, the findings illustrated in Fig. 3 suggest that drops at these conditions would not necessarily shatter due to small surface tension as often thought;[2] instead, they would deform or even remain spherical. However, additional study of such high pressure drop processes is needed before definitive conclusions about this behavior can be obtained. In particular, specific drop trajectories across the flow regime map depend on atomization and mixing properties of the spray while near-critical drop processes involve much lower values of ρ_f/ρ_g than those considered in Fig. 3.

All the regime transitions illustrated in Fig. 3 become relatively independent of liquid viscous forces (or Oh) for Oh < 0.01. The We for regime transitions in this low Oh regime are summarized in Table 2, considering results from Hinze,[6] Krzeczkowski[17] and the present study. Similar to the regime map itself, the measurements of the various studies agree within experimental uncertainties. The order of the transitions with increasing We is as follows: nonoscillatory deformation, oscillatory deformation, bag breakup, bag-jet breakup (defined as a separate regime in Ref. 17 but not during the present study), multimode breakup (which involves evolution from center to edge deformation of the drop and is called transition breakup in Ref. 17) and finally shear breakup. Catastrophic breakup occurs for We > 10^4, which is beyond the present test range.

Breakup Times

The discussion of deformation and breakup regime transitions highlights the importance of breakup times. In particular, as drop velocity relaxation times and breakup times approach one another, the propensity for drop breakup decreases due to reduction of relative velocities between the drop and the gas. Present measurements of breakup times, along with earlier measurements for shock wave disturbances due to Engel,[8] Simpkins and Bales,[13] Ranger and Nicholls,[18] and Reinecke and coworkers,[19,20] are illustrated in Fig. 4. The breakup times in the figure are normalized by the characteristic breakup time for shear breakup defined by Ranger and Nicholls[18] as follows:

$$t^* = d_o(\rho_f/\rho_g)^{1/2}/u_o \qquad (1)$$

with t_b/t^* plotted as a function of We. Except for the present results, which are grouped according to Oh, the measurements are for Oh < 0.1 and effects of liquid viscosity are small. Thus, the deformation and breakup regimes at small Oh identified in Table 2 are illustrated on the figure for reference purposes (omitting catastrophic, etc., breakup regimes at high We, as noted earlier).

A remarkable feature of the breakup time results of Fig. 4 at Oh < 0.1 is that t_b/t^* varies very little even though We varies over a large range (roughly 10-10^6) and a variety of breakup regimes are involved. In fact, the breakup time correlation of Ranger and Nicholls,[18] developed for the shear breakup regime

$$t_b/t^* = 5.0 \qquad (2)$$

provides a reasonably good correlation of all the measurements illustrated in Fig. 4. However, when present results for Oh > 0.1 are considered, it is seen that t_b/t^* progressively increases with increasing Oh. This reflects the importance of liquid viscosity on breakup evident from the breakup regime map of Fig. 3; in particular, large Oh involves eventual suppression of breakup so that t_b/t^* becomes unbounded. An empirical fit of this behavior over the present test range is as follows:

$$t_b/t^* = 5/(1\text{-}Oh/7); \quad We < 10^3 \qquad (3)$$

Equation (3), however, is only provisional because it is based on relatively few data with Oh generally less than 3.5.

Drop Deformation

The first stage of drop deformation, in the period where the drop flattens and first reaches a maximum crosstream

dimension, was studied due to its influence on drop velocity relaxation and breakup. In particular, the distortion of the drop should affect its drag properties, and thus relative velocities during the breakup process, which undoubtedly plays a role in the onset of breakup. Experimental uncertainties (95% confidence) of present measurements of drop dimensions in this period are estimated to be less than 5%.

Measurements of the crosstream distortion of the drops, d_c-d_o, normalized by the maximum crosstream distortion, are plotted as a function of t/t^* in Fig. 5. All these results are for Oh < 0.1, where effects of liquid viscosity on breakup times are small. Results of Ranger and Nicholls[18], for breakup at We > 10^4, are shown on the figure along with present results in the deformation and bag breakup regimes, to represent behavior at the limits of the breakup process.

When normalized in the manner of Fig. 5, drop distortion correlates reasonably well as a linear function of time. The maximum distortion is reached at roughly $t/t^* = 1.6$, or at roughly 30% of the total breakup time. Notably, measurements discussed by Gel'fand et al.[14] for a similar range of conditions, and plotted by Wierzba and Takayama[21] for the shear breakup regime, exhibit very similar behavior. However, the very high Weber number measurements of Reinecke and Waldman[20] (We > 10^6) exhibit somewhat delayed growth to d_{cmax}. These findings suggest that scaling of drop distortion in the early stages of breakup is relatively universal for We < 10^5, which includes the deformation, bag breakup and shear breakup regimes: this is in general agreement with effects of We and breakup regime on the breakup times discussed in connection with Fig. 4.

As might be expected, measurements of drop distortion at Oh > 0.1, show progressive delay in the time required for the drop to reach maximum distortion. In fact, this behavior is very similar to effects of Oh on breakup time so that results like to Fig. 5 can be obtained in terms of a corrected characteristic breakup time

$$t_c^* = t^* / (1\text{-}Oh / 7) \qquad (4)$$

over the present test range (We < 10^3, Oh < 3.5).

The next parameter of interest is the maximum crosstream diameter of the drop, d_{cmax}. An approximate expression for the variation of d_{cmax} with flow conditions can be obtained for conditions where effects of liquid viscosity are small, Oh < 0.1, by considering the interaction between surface tension and pressure forces when the drop is drawn into a flattened shape. For this treatment, the following assumptions are made: neglect variations in the relative velocity up to the time d_{cmax} is reached are neglected; the pressure difference between the bulk of the drop liquid and the region near the edge of the drop is assumed to be proportional to the dynamic head of the flow, $\rho_g u_0^2 / 2$; surface tension forces are assumed to act near the periphery of the deformed (ellipsoidal shaped) drop, along a perimeter of length πd_{cmax} to resist the pressure forces; and the pressure forces are assumed to act across a peripheral crossectional area $\pi d_{cmax} d_{smin}$, where d_{smin} is the streamwise diameter of the drop along its axis when d_{cmax} is reached. Equating these forces yields:

$$2 \sigma \pi d_{cmax} = C_f \pi d_{cmax} d_{smin} \rho_g u_0^2 / 2 \qquad (5)$$

where C_f is an empirical coefficient of order of magnitude unity to allow for effects of the actual pressure distribution and shape of the drop. During the period of deformation, the total volume of the drop is conserved; thus, assuming that the deformed drop is an ellipsoid about its flow axis, there results:

$$d_{smin} d^2_{cmax} = C_v d_o^3 \qquad (6)$$

where C_v is an empirical coefficient of order of magnitude unity to allow for departures of the drop from an ellipsoidal shape. Eliminating d_{smin} between Eqs. (5) and (6) then yields

$$d_{cmax} / d_o = (C_f C_v / 2)^{1/2} We^{1/2} \qquad (7)$$

accounting for the fact that d_{cmax} / d_o approaches unity as We becomes small, and fitting the empirical constant using the present measurements, finally yields:

$$d_{cmax} / d_o = (d_{smin} / d_o)^{-1/2} = 1 + 0.19\ We^{1/2},\ Oh < 0.1,$$
$$We < 10^2 \qquad (8)$$

where the second part of Eq. (8) follows from Eq. (5) taking $C_v = 1$ (which was representative of present measurements).

Figure 6 is an illustration of present measurements of d_{cmax} / d_o as a function of We, with Oh as a parameter. The correlating expression of Eq. (8) for Oh ≤ 0.1 also is plotted on the figure. It is evident that Eq. (8) provides a reasonable fit of the data, however, it should be noted that Eq. (8) is slightly inconsistent with the transition to the nonoscillatory deformation regime of Fig. 3 because it somewhat overestimates d_{cmax} / d_o near We = 1 (by roughly 10%). Effects of increasing Oh can be seen, with d_{cmax} / d_o tending to decrease at a particular We as Oh is increased. Because the deformation motions of the drop cease at the point where d_{cmax} is reached, this behavior is not thought to be a direct effect of viscous forces on the force balance fixing d_{cmax}. Instead, the increased time of deformation due to effects of liquid viscosity is a more probable mechanism. This allows drag forces to act for a longer time before the maximum deformation condition is reached, which tends to reduce the relative velocity, and correspondingly d_{cmax} through Eqs. (5) and (6). This effect also must be responsible for the increased We required for transition to the nonoscillatory deformation regime as Oh increases, seen in Fig. 3. To initiate work toward quantifying this mechanism, the drag properties of drops as they deform will be taken up next.

Drop Drag

Drop drag properties were found by measuring the motion of the centroid of the drop in the uniform flow field behind the shock wave. This approach is only approximate because it neglects the forces involved as the mass of the drop is redistributed during drop deformation. However, this effect is not expected to be large for present test conditions because characteristic velocities in the liquid phase are small. For example, considering either the normal motion of liquid along the axis due to the static pressure increase near the forward stagnation point, or the acceleration of the liquid as the local static pressure decreases in moving toward the edge of the deformed drop, yields the following characteristic liquid phase velocity:

$$u_f = (\rho_g / \rho_f)^{1/2} u_o \qquad (9)$$

For present conditions u_f / u_o is in the range 0.03 - 0.04, so that the motion of the drop as a whole should dominate drag properties. Additionally, pressure gradient forces are negligible because the flow behind the shock wave is uniform, and virtual mass and Basset history forces can be neglected because $\rho_g / \rho_f << 1$.[26]

The drop drag coefficient was defined in terms of the local relative velocity and crosstream dimension of the drop as follows:

$$C_D = D / (\pi d_c^2 \rho_g u^2 / 8) \qquad (10)$$

Under present assumptions only the acceleration of the drop must be considered when evaluating the drag force, yielding the following expression for C_D from the measurements of centroid position, x, as a function of time:

$$C_D = 2\rho_f d_o^3 \, dx^2 / dt^2 / (3\rho_g d_c^2 (u_o - dx / dt)^2) \quad (11)$$

The measurements of C_D primarily were limited by the accuracy of defining centroid motion at small times after passage of the shock wave, to yield experimental uncertainties (95% confidence) less than 30%.

The experiments to find C_D involved the initial deformation of the drops up to the time d_{cmax} was reached, Oh < 0.1 and a moderate range of Reynolds numbers (1000-2500) where effects of Reynolds number on the drag of the drops are expected to be small.[26] Thus, it was found that C_D largely was a function of the degree of deformation of the drop for present test conditions. In order to highlight this behavior, the results are plotted in terms of d_c / d_o in Fig. 7. Measurements of C_D for solid spheres and thin disks, drawn from White[27] for the same range of Re as the present tests, also are illustrated on the plot. In spite of the relatively large uncertainties of the measurements, the trend of the data is quite clear; for d_c / d_o near unity, C_D approximates results for solid spheres and then increases to approach results for thin disks at $d_c / d_o \approx 2$. Thus, behavior in the period observed appears to be dominated by distortion of the drop, rather than internal circulations which would cause reductions of C_D from values appropriate for solid spheres. This seems reasonable because characteristic liquid phase velocities are relatively small for present test conditions, cf., Eq. (9).

Drop Sizes

Measurements of drop sizes after breakup were limited to conditions where Oh < 0.1. This was necessary in order to capture the entire drop field after breakup on a single hologram, because larger values of Oh yielded regions containing drops that were too large for the present optical arrangement. The measurements included We < 10^3, which corresponds to the bag, transition and shear breakup regimes.

Past work on the structure of dense sprays and processes of primary breakup of nonturbulent and turbulent liquids,[1-4] indicated that local drop size distributions generally satisfied the universal root normal distribution function of Simmons,[28] with MMD / SMD = 1.2. This vastly simplifies the presentation of data because the root normal distribution only has two moments and with MMD / SMD a constant is entirely specified by the SMD alone. Thus, initial measurements of drop sizes after breakup focussed on evaluating the root normal distribution function.

Some typical measurements of drop size distributions, involving water drops with We in the range 15-125, are illustrated in Fig. 8. The results are plotted in terms of the root normal distribution function, with the function itself illustrated for values of MMD / SMD = 1.10, 1.20 and 1.50. The results are somewhat scattered at large drop sizes because the number of large drops is limited from breakup of single drops; and at small drops sizes, due to difficulties in finding and resolving the smallest drops in the distribution. In view of these effects, the drop size distributions are reasonably represented by the universal root normal distribution function with MMD / SMD = 1.2, similar to the findings of Refs. 1-4. This is perhaps not surprising because drops within dense sprays have generally undergone secondary breakup and satisfy this distribution function on a local basis as well.[1] On the other hand, Gel'fand et al.[14] observe a bimodal distribution of drop sizes after bag breakup for the two conditions they consider. However, evidence of bimodal behavior was not observed for any of the present measurements. The reason for this discrepancy is unknown and clearly merits additional study.

A correlating expression for the SMD after secondary breakup can be obtained by noting the similarity of primary breakup of nonturbulent liquids and shear breakup of drops. In both cases, drops or ligaments are stripped from boundary layers in the liquid phase that form near the liquid surface: on the windward side of waves along the surface for primary breakup of nonturbulent liquids,[3] and on the windward side of the drop for secondary breakup in the shear breakup regime. It is assumed that the relative velocity at the time of breakup can be represented by the initial relative velocity, u_o, and that drop sizes after breakup are comparable to the thickness of the boundary layer as it reaches the periphery of the drop, i.e., that liquid is stripped from the periphery of the drop which is observed in this breakup regime. Since this boundary layer develops while moving away from the forward stagnation point of the flow, the characteristic velocity in the liquid phase is taken as u_f from Eq. (9). Additionally, the SMD is dominated by the largest drop sizes in the distribution so that the length of development of the liquid boundary layer is taken to be proportional to d_o, which should be the condition tending to yield the largest drop sizes. Finally, assuming that the boundary layer is laminar, due to the relatively small values of u_f and d_o, there results

$$SMD / d_o = C_s (\rho_f / \rho_g)^{1/4} [\mu_f / (\rho_f d_o u_o)]^{1/2} \quad (12)$$

where C_s is an empirical constant involving the various proportionality factors. It is convenient to rearrange Eq. (12) so that the Weber number based on SMD is obtained because this helps assess the potential for subsequent breakup of the largest drops in the distribution. Completing this rearrangement yields:

$$\rho_g \, SMD \, u_o^2 / \sigma = C_s (\rho_f / \rho_g)^{1/4} [\mu_f / (\rho_f d_o u_o)]^{1/2} \, We \quad (13)$$

Present measurements of SMD after secondary breakup are plotted in terms of Eq. (13) in Fig. 9. These results are for Oh < 0.1 and We < 10^3, including the bag, transition and shear breakup regimes. A correlation of the data also is shown on the plot. The power of this correlation is unity, in agreement with Eq. (13) within experimental uncertainties, yielding the following empirical fit:

$$\rho_g \, SMD \, u_o^2 / \sigma = 6.2 (\rho_f / \rho_g)^{1/4} [\mu_f / (\rho_f d_o u_o)]^{1/2} \, We \quad (14)$$

The standard deviations of the coefficient and the overall factor on the right hand side of Eq. (14) are 20 and 10%, respectively, with the correlation coefficient of the fit being 0.91. It should be noted, however, that ρ_f / ρ_g does not vary greatly over the present test range and additional measurements are needed to explore density ratio effects.

Several effects are of interest in connection with the results illustrated in Fig. 9. First of all, it is surprising that a single correlation can express the SMD after bag, transition and shear breakup because the mechanisms appear to be rather different. However, this behavior is consistent with the observations that breakup times correlated in a similar manner for the three breakup regimes, as discussed in connection with Fig. 4. Additionally, the largest drops formed during bag breakup come from the ring at the base of the bag, which has similar length and velocity scales, u_f and d_o, during its formation. Thus, similarity of SMD after breakup for the bag and shear breakup regimes, with related behavior for the transition regime that separates them, seems reasonable based on these considerations.

A second effect seen in Fig. 9 is that the measurements for different liquids clearly separate in a systematic manner. Thus the slopes of the curves, which are largely governed by the values of u_o and d_o used during the experiments, are represented quite well by Eq. (14) but the intercepts vary with the liquid. Since the density ratios and surface tensions do not vary greatly over the present test range, the effect is largely due to changes of liquid viscosity. The main effect is that Eq. (14) overestimates the effect of liquid viscosity, with more viscous liquids systematically shifted to the right. The reason for this behavior is unknown at present; until the issue is resolved it is recommended that Eq. (14) only be used for liquids having viscosities within the range of present measurements.

A third effect with respect to the results illustrated in Fig. 9 involves the propensity of the largest drops in the distribution after breakup to undergo additional breakup. In order to assess the potential for additional deformation and breakup, the regime transitions at low Oh from Table 2 have been drawn on the plot (interpreting the ordinate as the We number of particular drops in the distribution after breakup and assuming that u_o is still representative of the relative velocity). Noting that more half the mass of the spray involves drop diameters greater than the SMD (MMD/SMD = 1.2), it is clear that a significant fraction of the drops after secondary breakup are in the deformation and bag breakup regimes. Additionally, the largest drops after secondary breakup (99.7% of the spray mass involves drop diameters less than 3.5 SMD) would reach the multimode breakup regime for present test conditions, with potential for shear breakup at higher drop Weber numbers. Naturally, these estimates are based on the assumption that the largest drops after secondary breakup have relative velocities near u_o, which must still be assessed by measurements of the correlation between drop sizes and velocities after secondary breakup. Work along these lines, as well as to better resolve effects of density ratio and liquid viscosity on drop breakup properties, has been initiated in this laboratory.

Conclusions

Drop deformation and secondary breakup after a shock wave initiated disturbance were studied, considering drops of water, n-heptane, mercury and various glycerol mixtures in air at normal temperature and pressure (We of 0.5-1000, Oh of 0.0006-4, ρ_f / ρ_g of 580-12000 and Re of 300-16000). The major conclusions of the study are as follows:

1. Drop deformation and breakup occurs at We > 1 with the following deformation and breakup regimes identified (listed in order of appearance with increasing We): no deformation, nonoscillatory deformation, oscillatory deformation, bag breakup, multimode breakup and shear breakup. The We for onset of deformation and breakup regimes increases with increasing Oh, with no breakup observed over the present test range for Oh > 4 due to the stabilizing effect of liquid viscosity.
2. Unified temporal scaling of deformation and breakup processes was observed in terms of a characteristic breakup time that was nearly independent of We and tended to increase with increasing Oh, cf. Eqs. (1) and (4).
3. Drop drag coefficients evolved from the properties of spheres to those of thin disks as drop deformation progressed prior to breakup.
4. Drop size distributions after secondary breakup satisfied Simmons' universal root normal distribution function,[28] with MMD/SMD = 1.2, similar to recent observations of drop sizes in pressure-atomized sprays and after primary breakup,[1,3,4] and can be characterized by a single parameter like the SMD.
5. Drop sizes after secondary breakup decreased as We increased and could be correlated similar to recent results for primary breakup of nonturbulent liquids,[3] in terms of a characteristic liquid boundary layer thickness for all breakup regimes, cf. Eq. (14). Drop properties after secondary breakup at high We suggest potential for subsequent breakup of the largest drops in the size distribution.

Conclusions about the outcome of secondary breakup are limited to conditions where Oh < 0.1 and additional study at higher Oh is needed. In addition, practical sprays often involve lower values of ρ_f / ρ_g and Re than present experiments and anticipated effects of modifying these variables should be quantified.

Acknowledgements

This research was sponsored by the Air Force Office of Scientific Research, Grant No. 89-0516, under the technical management of J.N. Tishkoff. The authors also would like to thank C.W. Kauffman for loan of a major portion of the shock tube facility and advice concerning its operation. The U.S. Government is authorized to reproduce and distribute copies for governmental purposes notwithstanding any copyright notation thereon.

References

[1]Ruff, G.A., Wu, P.-K., Bernal, L. P. and Faeth, G.M., "Continuous and Dispersed-Phase Structure of Dense Nonevaporating Pressure-Atomized Sprays," J. Prop. Power, in press.

[2]Faeth, G.M. "Structure and Atomization Properties of Dense Turbulent Sprays," Twenty-Third Symposium (International) on Combustion, The Combustion Institute, 1990, Pittsburgh, pp. 1345-1352.

[3]Wu, P.-K., Ruff, G.A. and Faeth, G.M., "Primary Breakup in Liquid/Gas Mixing Layers," Atomization and Sprays, Vol. 1, No. 4, 1991, pp. 421-440.

[4]Wu, P.-K., Tseng, L.-K. and Faeth, G.M., "Primary Breakup in Gas/Liquid Mixing Layers for Turbulent Liquids," AIAA Paper No. 92-0462, 1992.

[5]Giffen, E. and Muraszew, A., The Atomization of Liquid Fuels, Chapman and Hall, Ltd., London, 1953.

[6]Hinze, J.O., "Fundamentals of the Hydrodynamic Mechanism of Splitting in Dispersion Processes," AIChE J., Vol. 1, No. 3, Sep. 1955, pp. 289-295.

[7]Lane, W.R., "Shatter of Drops in Streams of Air," Ind. Engr. Chem., Vol. 43, June 1951, pp. 1312-1317.

[8]Engel, O.G., "Fragmentation of Waterdrops in the Zone Behind an Air Shock," Journal of Research of the National Bureau of Standards, Vol. 60, No. 3, Mar. 1958, pp. 245-280.

[9]Hanson, A.R., Domich, E.G. and Adams, H.S., "Shock-Tube Investigation of the Breakup of Drops by Air Blasts," Phys. Fluids, Vol. 6, No. 8, Aug. 1963, pp. 1070-1080.

[10]Haas, F.C., "Stability of Droplets Suddenly Exposed to a High Velocity Gas Stream," AIChE J., Vol. 10, No. 6, Nov. 1964, pp. 920-924.

[11]Volynskii, M.S. and Lipatov, A.S., "Deformation and Disintegration of Liquid Drops in a Gas Flow," Inzhernerno-Fizecheskii Zhurnal, Vol. 18, No. 5, May 1970, pp. 838-843.

[12]Hassler, G., "Untersuchung zur Zerstörung von Wassertropfen durch Aerodynamische Krafte," Forsch. Ing. Wes., Vol. 38, No. 6, 1972, pp. 183-192.

[13]Simpkins, P.G. and Bales, E.J., "Water-Drop Response to Sudden Accelerations," J. Fluid Mech., Vol. 55, No. 4, 1972, pp. 629-639.

[14]Gel'fand, B.E, Gubin, S.A. and Kogarko, S.M., "Various Forms of Drop Fractionation in Shock Waves and their Special Characteristics," Inzhenerno-Fizicheskii Zhurnal, Vol. 27, No. 1, July 1974, pp. 119-126.

[15]Loparev, V.P., "Experimental Investigation of the Atomization of Drops of Liquid under Conditions of a Gradual Rise of the External Forces," Izvestiya Akademii Nauk SSSR, Mekhanika Zhidkosti i Gaza, No. 3, May-June 1975, pp. 174-178.

[16]Borisov, A.A., Gel'fand, B.E., Natanzon, M.S. and Kossov, O.M., "Droplet Breakup Regimes and Criteria for their Existence," Inzhenerno-Fizicheskii Zhurnal, Vol. 40, No. 1, Jan. 1981, pp. 64-70.

[17]Krzeczkowski, S.A., "Measurement of Liquid Droplet Disintegration Mechanisms," Int. J. Multiphase Flow, Vol. 6, 1980, pp. 227-239.

[18]Ranger, A.A. and Nicholls, J.A., "The Aerodynamic Shattering of Liquid Drops," AIAA J., Vol, 7, Feb. 1969, pp. 285-290.

[19]Reinecke, W.G. and McKay, W.L., "Experiments on Waterdrop Breakup Behind Mach 3 to 12 Shocks," Sandia Corp. Report SC-CR-70-6063, 1969.

[20]Reinecke, W.G. and Waldman, G.D., "A Study of Drop Breakup Behind Strong Shocks with Applications to Flight," Avco Report AVSD-0110-70-77, May 1970.

[21]Wierzba, A. and Takayama, K., "Experimental Investigation of the Aerodynamic Breakup of Liquid Drops," AIAA J., Vol. 26, No. 11, Nov. 1988, pp. 1329-1335.

[22]Liang, P.Y., Eastes, T.W. and Gharakhari, A., "Computer Simulations of Drop Deformation and Drop Breakup," AIAA Paper No. 88-3142, 1988.

[23]Dabora, E.K., "Production of Monodisperse Sprays," Rev. Sci. Inst., Vol. 38, April 1967, pp. 502-5-6.

[24]Sangiovanni, J. and Kestin, A.S., "A Theoretical and Experimental Investigation of the Ignition of Fuel Droplets," Combust. Sci. Tech., Vol. 16, No. 1 and 2, 1977, pp. 59-70.

[25]Lange, N.A., Handbook of Chemistry, 8th edition, Handbook Publishers, Inc., Sandusky, Ohio, 1952, pp. 1134 and 1709.

[26]Faeth, G.M., "Mixing, Transport and Combustion in Sprays," Prog. Energy Combust. Sci., Vol. 13, 1987, pp. 293-345.

[27]White, F.M., Viscous Fluid Flow, McGraw-Hill, New York, 1974, pp.

[28]Simmons, H.C., "The Correlation of Drop-Size Distributions in Fuel Nozzle Sprays," J. Engr. for Power, Vol. 99, July 1977, pp. 309-319.

Table 1 Summary of Test Conditions[a]

Liquid	ρ_f (kg/m^3)	$\mu_f \times 10^4$ (kg/ms)	$\sigma \times 10^3$ (N/m)	d_o (μm)	Oh (-)	We (-)	Re (-)
Water	997	8.94	70.8	1000	0.0038	0.5-236	342-8254
n-Heptane	683	3.94	20.0	500	0.0036	14-137	718-2270
Mercury	13600	15.0	475.0	850	0.00062	10-13	3510-4502
Solutions of glycerol:							
21%	1050	16.0	67.3	1200	0.0071	8-130	1542-6386
42%	1105	35.0	65.4	1200	0.0120	8-136	1530-6580
63%	1162	108.0	64.8	1200	0.0390	1-129	482-6420
75%	1195	356.0	63.8	1200	0.0990	2-128	730-6272
84%	1219	1000	63.2	1200	0.260	1-127	497-6214
92%	1240	3270	62.5	1200	1.050	1-268	531-8335
97%	1253	8350	62.4	1500	1.700	1-205	596-8876
99.5%	1260	12500	62.0	1550	3.850	1-612	632-15763

[a]Air initially at 98.8 kPa and 298± 3 K in driven section of shock tube with shock Mach numbers in the range 1.01-1.24. Properties of air taken at normal temperature and pressure: $\rho_g = 1.18$ kg/m^3, $\mu_g = 18.5 \times 10^{-6}$ kg/ms.

Table 2 Summary of We for Transition to Deformation and Breakup Regimes at Oh < 0.1

Transition to:	*Present*	*Krzeczkowski*[17]	*Hinze*[6]
Nonoscillatory Deformation	1.1	—	—
Oscillatory Deformation	3.0	—	—
Bag Breakup	13	10	13
Bag Jet Breakup	—	18	—
Multimode Breakup	35	30[a]	—
Shear Breakup	80	63	—

[a]Called transition regime in Ref. 17.

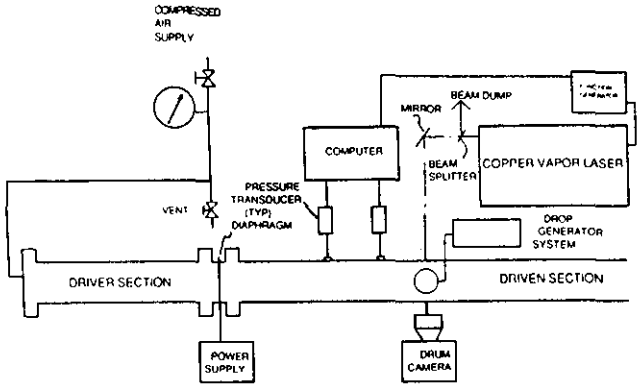

Fig. 1 Sketch of shock tube apparatus.

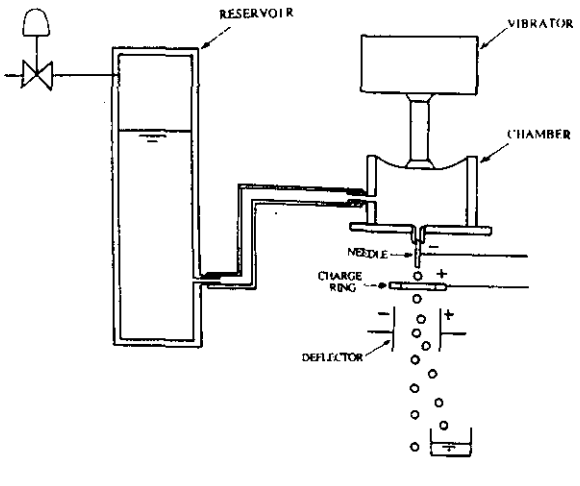

Fig. 2 Sketch of drop generator system.

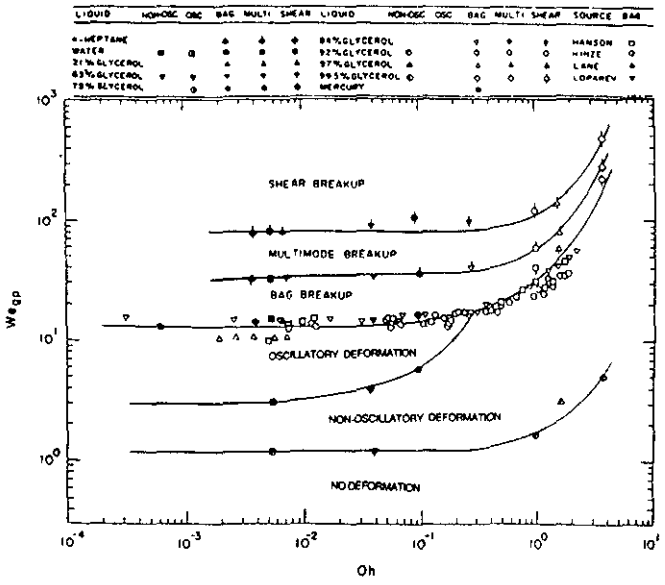

Fig. 3 Drop deformation and breakup regime map.

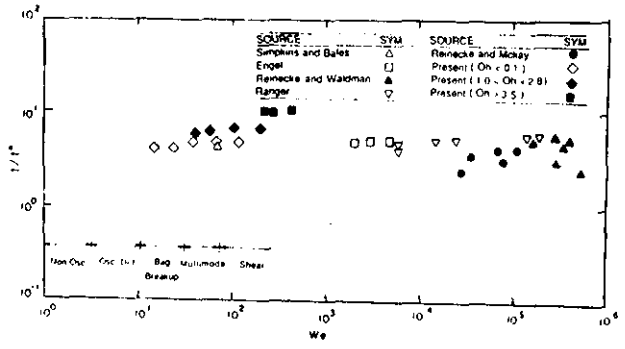

Fig. 4 Drop breakup times as a function of We and Oh.

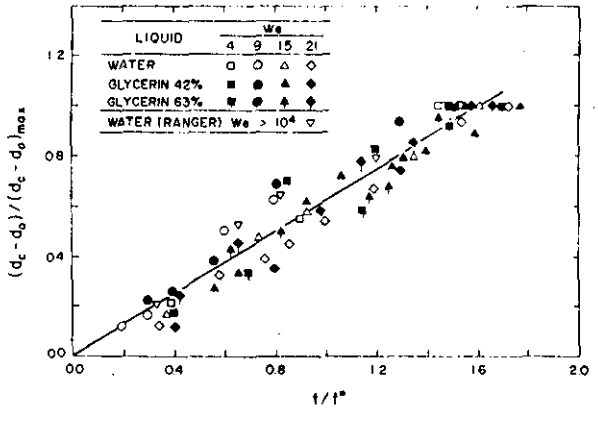

Fig. 5 Drop deformation prior to breakup as a function of normalized time.

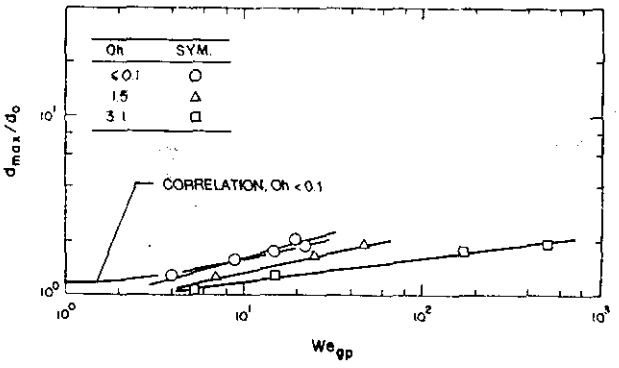

Fig. 6 Maximum crosstream drop diameters prior to breakup as a function of We and Oh.

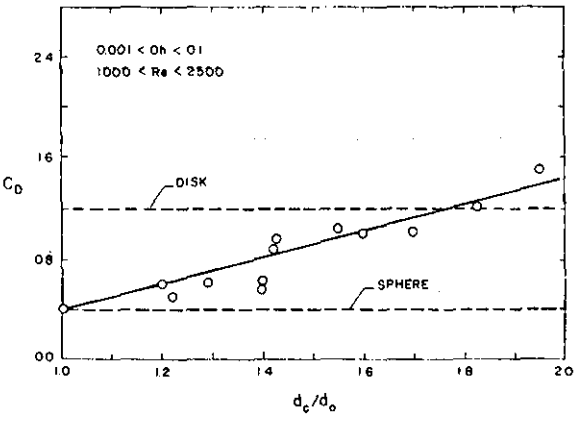

Fig. 7 Drop drag coefficient prior to breakup as a function of normalized crosstream diameter.

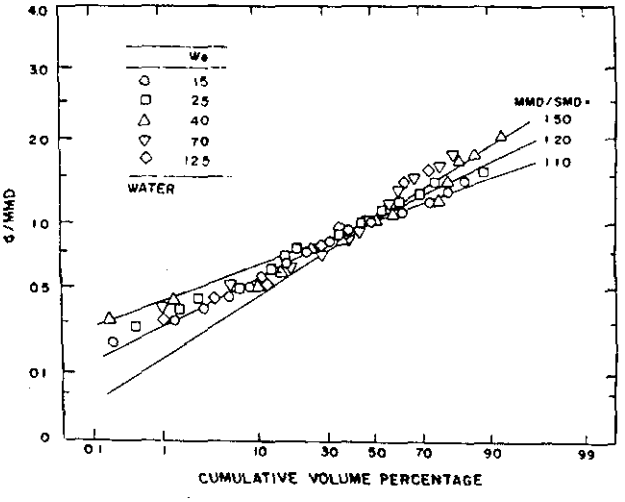

Fig. 8 Distribution of drop diameters after breakup.

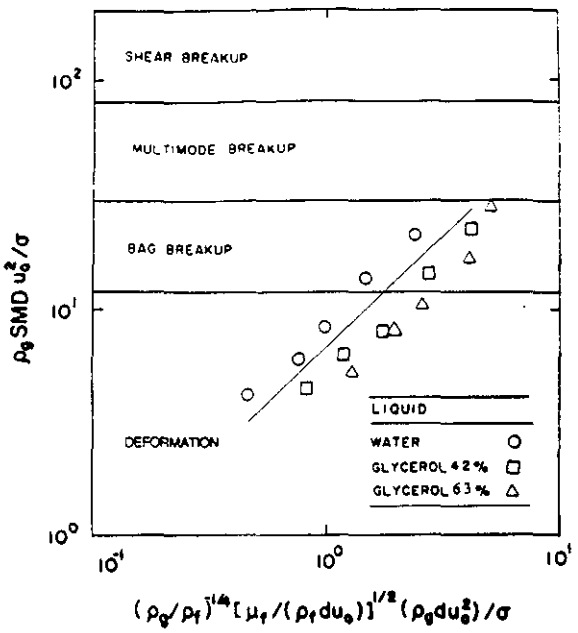

Fig. 9 Correlation of SMD after secondary breakup.